Applied Catalysis B: Environmental 92 (2009) 23–29

Contents lists available at ScienceDirect

Applied Catalysis B: Environmental

journal homepage: www.elsevier.com/locate/apcatb

Improved NO_x storage-reduction catalysts using Al_2O_3 and ZrO_2–TiO_2 nanocomposite support for thermal stability and sulfur durability

Haruo Imagawa *, Naoki Takahashi, Toshiyuki Tanaka, Shin'ichi Matsunaga, Hirofumi Shinjoh

Toyota Central Research and Development Labs, Inc., 41-1 Yokomichi, Nagakute, Nagakute-cho, Aichi 480-1192, Japan

ARTICLE INFO

Article history:
Received 28 March 2009
Received in revised form 25 July 2009
Accepted 28 July 2009
Available online 5 August 2009

Keywords:
Nanocomposite
Thermal stability
Sulfur durability
NO_x storage-reduction catalyst

ABSTRACT

A nanocomposite of Al_2O_3 and ZrO_2–TiO_2 solid solution (AZT) was synthesized for NO_x storage-reduction (NSR) catalysts Pt/Rh/Ba/K/AZT, and the effect of calcination temperature on thermal stability was investigated. The catalyst containing AZT calcined at 1073 K (AZT catalyst) had a high NO_x storage capacity after thermal aging. This enhanced storage capacity was attributed to the fact that ZrO_2–TiO_2 solid solution (ZT) was crystallized and stabilized. The solid-state reaction of potassium, which was added as a NO_x storage material, was inhibited in the AZT catalyst, relative to those containing AZT calcined at a low temperature. The AZT catalyst also showed excellent NO_x storage performance after sulfur aging at 973 K or higher, compared with the catalyst containing physically mixed Al_2O_3 and ZT (physically mixed catalyst). Furthermore, AZT catalysts inhibited the solid phase reaction of potassium with support materials and kept a high ratio of active potassium, which can store NO_x. Further, because the barium in the AZT catalyst prevented sulfur poisoning, the ratio of active barium in the AZT catalyst was also larger than that in the physically mixed catalyst, probably because of the low basicity and high Pt dispersion of AZT.

1. Introduction

The lean-burn engine is a promising means for reducing carbon dioxide (CO_2) emissions from automobiles. However, since lean-burn combustion produces excess oxygen in the process of combustion, conventional three-way catalysts cannot completely reduce nitrogen oxides (NO_x) to nitrogen (N_2) under lean conditions. To overcome this problem, a variety of catalysts for reducing NO_x in lean systems have been investigated [1–4].

The NO_x storage-reduction catalyst (NSR catalyst) is one of the most attractive methods for reducing NO_x emissions from lean-burn engines [5,6]. The NSR catalyst operates according to the following reaction mechanism [7]: First, excess NO_x is oxidized to NO_2 on precious metal catalysts and stored in the form of nitrate in the storage materials. When the engine operation is switched to a rich air–fuel ratio, the nitrates stored in the storage material are reduced to N_2 by hydrogen (H_2), carbon monoxide (CO), and hydrocarbons (HCs).

The NSR catalyst has two technical disadvantages: sulfur poisoning and thermal deterioration. Sulfur poisoning is caused by sulfur dioxide (SO_2) in the exhaust gas. SO_2 adsorbs onto the catalysts and reacts with the storage materials, forming sulfate salts, and the NO_x storage materials can no longer store NO_x. Consequently, the effect of sulfur on storage materials has been extensively investigated [8–14]. Recent studies on sulfur durability in catalysts have reported that TiO_2 in support materials provides high tolerance against sulfur poisoning due to the high acidity/low basicity of TiO_2 [8,15–17]. Furthermore, TiO_2 is used in the fabrication of ZrO_2–TiO_2 solid solution (ZT) to prevent the solid phase reaction of the NO_x storage materials with TiO_2 upon heating [7,16]. ZT has also been shown to have low basicity for sulfur durability without losing TiO_2 properties [7,17]. Al_2O_3 is indispensable in automobile catalysts because of its excellent thermal stability; however, since it tends to adsorb SO_2 due to its high basicity, the addition of TiO_2 to Al_2O_3 has been investigated in order to prevent SO_2 from adsorbing on the catalyst surface [18]. TiO_2 doped Al_2O_3 with sulfur resistance is thus an important consideration affecting the sulfur durability of the NSR catalyst.

Thermal deterioration of the catalyst is not only caused by the aggregation of support materials and precious metals [19], but also by the solid phase reaction of the NO_x storage materials [20,21]. Recently, we developed a novel nanocomposite of Al_2O_3 and ZT (AZT) as a support material [22]. In this nanocomposite, primary Al_2O_3 and ZT particles coexist within the same secondary particle. AZT has been found to inhibit the thermal aggregation of ZT, because Al_2O_3 acts as a diffusion barrier to ZT particles in secondary particles (Fig. 1). Therefore, the particle growth of ZT as well as the sintering of precious metals on the supports can be prevented. In addition, since AZT has been shown to have low basicity due to the presence of a small amount of TiO_2 in Al_2O_3 [18],

* Corresponding author. Tel.: +81 561 71 7226; fax: +81 561 63 5743.
E-mail address: e1152@mosk.tytlabs.co.jp (H. Imagawa).

0926-3373/$ – see front matter © 2009 Elsevier B.V. All rights reserved.
doi:10.1016/j.apcatb.2009.07.027

the NSR catalyst containing AZT as a support material exhibits both higher sulfur durability and excellent thermal stability.

However, in order to further improve the NSR catalyst, it is necessary to confirm the mechanism of the superior NSR performance using AZT with an ideal structure. Although basic characterization of AZT as a support has been already carried out in the previous report [22], detailed characterization of AZT catalyst for NSR reaction has not yet been conducted. Investigation of the relationship between supports and NO_x storage materials after aging tests will lead to new findings not only for thermal stability, but also for sulfur durability.

The purpose of this investigation was to analyze and improve the thermal stability and sulfur durability of the NSR catalyst using AZT. This paper consists of two topics. In the first section, the effect of the calcination temperature of AZT on thermal stability was investigated. In the second section, a monolithic catalyst containing AZT after sulfur aging at high temperature was analyzed through the analysis of storage materials. The evaluation of catalysts using a monolithic substrate is a useful method for determining the practicability of a real NSR catalyst. These findings are of particular interest for determining the state of NO_x storage materials.

2. Experimental

2.1. Preparation of supports

AZT was prepared using a conventional co-precipitation method [22], with the mole ratio for Al_2O_3:ZrO_2:TiO_2 being 50:30:20 (mol%). The obtained powder was calcined at 773, 873, 973, 1073, and 1173 K for 5 h, and is referred to herein as AZT*n* (*n* = 773, 873, 973, 1073, and 1173).

Pure γ-Al_2O_3 was prepared using the same method described for AZT [22], and pure ZT was prepared as described in the literature [7]. A reference support was obtained by physically mixing pure γ-Al_2O_3 and ZT (physically mixed oxide). The composition of the physically mixed oxide was the same as that of AZT.

The Brunauer–Emmett–Teller (BET) surface area of AZT*n* was measured by N_2 adsorption at 77 K using an automatic surface area analyzer (Micro Data, Micro Sorp 4232II). The crystal structures of AZT*n* and pure ZT were characterized by powder X-ray diffraction (XRD). XRD patterns were recorded using an X-ray diffractometer (Cu Kα radiation λ = 1.5418 Å, 40 kV, 30 mA) (Rigaku, RINT-2100). The particle size of ZrO_2–TiO_2 was calculated using Scherrer's formula [23]. The peak at $2\theta = 30.4^\circ$, assigned to the tetragonal ZrO_2 (1 0 1) phase, was used to calculate the particle size of ZT.

The base surface properties of the supports were measured using CO_2-temperature programmed desorption (CO_2-TPD). Samples were formed into 0.3–0.7 mm diameter pellets. The CO_2-TPD samples were pretreated at 773 K in a helium (He) atmosphere. After the samples had been exposed to CO_2 under a stream of He at 373 K, they were heated to 773 K at a rate of 20 K/min. CO_2 desorbed from samples in a He atmosphere was observed using a non-dispersive infrared (NDIR) analyzer attached to an exhaust gas analyzer (Horiba, MEXA-7100).

2.2. Effect of AZT calcination temperature on thermal stability

Pellet catalysts were prepared by impregnating $Pt(NH_3)_2(NO_2)_2$ and $Rh(NO_3)_3$ (Tanaka Precious Metals) with the AZT prepared in Section 2.1, drying at 383 K for 12 h, and finally calcining at 523 K for 3 h in air. The Pt and Rh loadings were 1.23 and 0.06 wt%, respectively. The powder obtained was then added to an aqueous solution containing $(CH_3COO)_2Ba$ and CH_3COOK (Wako Pure Chemical Industries) as precursors to the storage materials. The Ba (BaO) and K (K_2O) loadings were 18.8 and 5.8 wt%, respectively. After the catalysts were dried at 383 K for 12 h, they were calcined at 773 K for 3 h in air. The powder obtained was formed into 0.3–0.7 mm diameter pellets, resulting in the catalyst using AZT*n* being referred to as the pelletized AZT*n* catalyst (P-AZT*n*Cat).

For thermal aging, the fresh pelletized catalysts were exposed to a feed-stream, as shown in Table 1. The stream simulated actual engine exhaust gas, and was heated at 1073 K for 5 h. The lean and rich atmospheres were cycled at 2 min intervals using a flow rate of 1000 cm^3/min and a gas hourly space velocity (GHSV) of 30 000 h^{-1}.

The sulfur-aging tests for the fresh pelletized catalysts were carried out at 873 K in a sulfur-containing atmosphere for the two gas compositions shown in Table 1. The lean and rich atmospheres were alternated every 30 s, and a gas flow rate of 4000 cm^3/min and a GHSV of 240 000 h^{-1} were used. The mole ratio of SO_2 to storage materials was S/(Ba + 0.5K) = 1.5.

The amount of NO_x stored in the aged pelletized catalysts was measured using a conventional fixed-bed flow reactor system at atmospheric pressure. Table 1 shows the composition of the feed-streams used to simulate actual engine exhaust gases for this measurement. Overview of the measurement is shown in Fig. 2. After 0.5 g of the pelletized catalyst was heated to 573 K under the rich atmosphere condition, the gas was switched to the lean

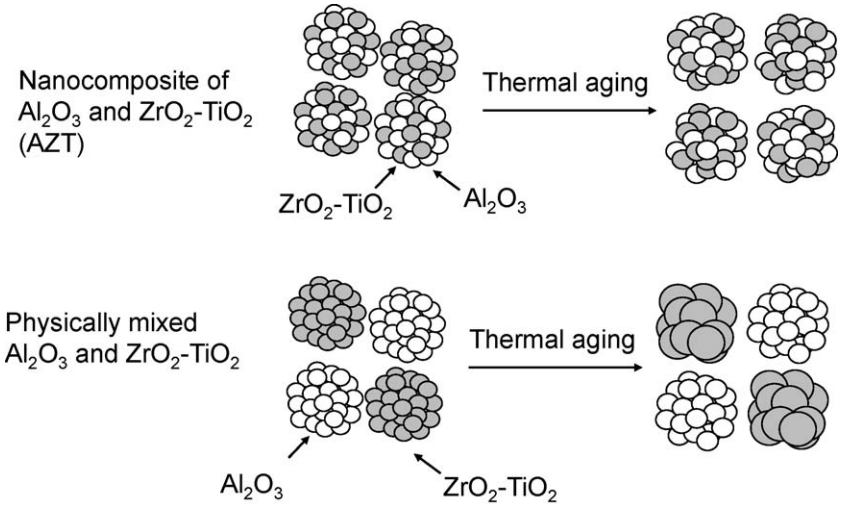

Fig. 1. Concept chart for AZT.

Table 1
Gas composition for thermal and sulfur-aging test, and NO_x storage measurement for pelletized catalysts.

Atmosphere	C_3H_6 (%C)	CO (%)	H_2 (%)	NO (ppm)	CO_2 (%)	SO_2 (ppm)	O_2 (%)	H_2O (%)
Thermal aging test[a]								
Lean	0.065	0	0	800	11	0	6.6	3
Rich	0.34	5.6	1.9	50	11	0	0	3
Sulfur-aging test[a]								
Lean	0.15	1.43	0.47	800	9.6	480	7.7	3
Rich	0.16	4.5	1.5	50	10	500	0	3
NO_x storage measurement[b]								
Lean	0.02	0	0	800	11	0	6.6	3
Rich	0.11	5.6	1.9	0	11	0	0.3	3
Rich spike	0.11	5.6	1.9	50	11	0	0	3

[a] N_2 balance.
[b] He balance.

atmosphere condition until the outlet NO_x concentration became constant, and then the catalyst was exposed to a 3 s rich spike. During rich spike injection, NO_x storage sites are regenerated, and the gas was subsequently switched to the lean atmosphere until the outlet NO_x concentration became constant. The amount of NO_x stored was calculated as the difference in NO_x between the inlet and the outlet gases after introduction of the rich spike (shaded area in Fig. 2). The molar amount of total reducing agents during a 3 s rich spike is more than that of all NO_x storage sites, given NO_x storage materials form $Ba(NO_3)_2$ and KNO_3.

The amounts of NO_x stored at 673 and 773 K were measured in the same manner as for 573 K, and these measurements were carried out sequentially after the experiment at 573 K. The gas flow rate was 3000 cm^3/min and the GHSV was 180 000 h^{-1}. The NO_x concentration was measured using a chemiluminescence NO_x meter attached to a gas exhaust analyzer (Horiba, MEXA-7100).

The state of potassium in the pelletized catalysts was analyzed using an inductively coupled plasma emission (ICP) spectrometer (Rigaku, CIROS 120EOP) as described elsewhere in the literature [7].

2.3. Analysis of the AZT catalyst for sulfur durability

A 7 g quantity of support powder was wash-coated on a hexagonal cell cordierite monolithic substrate (62 cells/cm^2) with a diameter of 30 mm and a length of 50 mm. AZT1073 was selected as a support, and a physically mixed oxide was used as a reference support. Catalysts were prepared by impregnating $Pt(NH_3)_2(NO_2)_2$ and $Rh(NO_3)_3$, drying at 383 K for 12 h, and finally calcining at 573 K for 3 h in air. The amounts of Pt and Rh were 0.8 and 0.2 wt%, respectively. The coated substrates were then added to an aqueous solution containing $(CH_3COO)_2Ba$ and CH_3COOK as precursors of the storage materials. The Ba (BaO) and K (K_2O) loadings were 12.8 and 2.9 wt%, respectively. Once catalysts had been dried at 383 K for 12 h, they were calcined at 573 K for 3 h in air. The catalyst using AZT1073 as a support is referred to as the monolithic AZT catalyst, and that using the physically mixed oxide is referred to as the physically mixed catalyst in Section 3.2.

Sulfur aging of the monolithic catalysts at high temperature was carried out at 973, 1023, and 1073 K for 5 h under a sulfur-containing atmosphere (Table 2). The 110 s lean and the 10 s rich atmospheres were then cycled alternately for the duration of the aging test. The gas flow rate was 10 000 cm^3/min and the GHSV was 17 140 h^{-1}.

As described in Section 2.2, the amount of NO_x stored on the aged monolithic catalysts was measured in the same manner as that at 673 K, under the gas composition shown in Table 2. The gas flow rate was 30 000 cm^3/min and the GHSV was 51 500 h^{-1}. The gas composition and gas flow rate in this measurement is slightly modified based on that for pelletized catalysts shown in Section 2.2 in order to reflect more practical condition suited for monolithic catalysts [21,24]. The NO_x concentration was measured using a chemiluminescence NO_x meter attached to a gas exhaust analyzer (Best Sokki, CATA-5000).

The residual amount of sulfur in the sulfur-aged monolithic catalysts was measured using a combustion infrared absorption analyzer (Horiba, EMIA-1200). After the sulfur-aging test, mapping of the residual S in the wash-coat layer was carried out by electron probe micro analysis (EPMA) using an electron probe micro analyzer (Shimadzu, EPMA-V6). The ratio of S to Ba in the sulfur-aged AZT catalyst powder was analyzed using an energy-dispersive X-ray (EDX) analyzer equipped with a field-emission transmission electron microscope (Hitachi, HF-2000). The diameter of the EDX analysis area was approximately 10 nm. The analyzed part contained a Pt particle and neighboring barium species. The ratio of S to Ba was observed as a function of the distance from a Pt particle. The state of the storage material was analyzed using the same method as that described in Section 2.2. The states of the potassium species were as follows: the active state, K_2CO_3, the sulfate state, K_2SO_4, and the solid phase-reacted state with support materials, mainly TiO_2 [7]. The barium species were classified as the active state, $BaCO_3$, and the other states, including the sulfate-formed state and the solid phase-reacted state, as described in the literature [8].

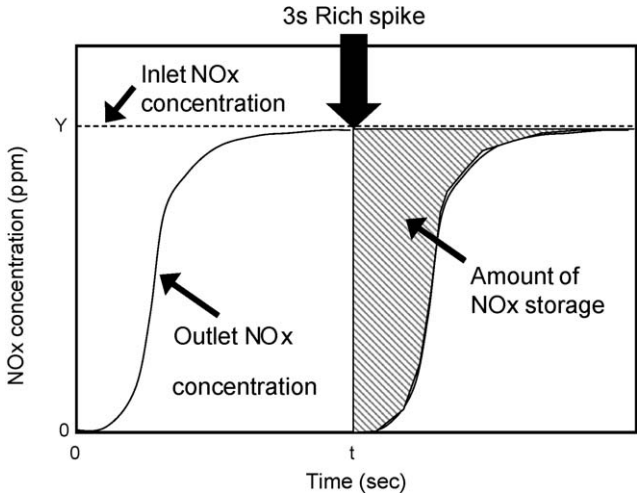

Fig. 2. Measurement of the amount of NO_x storage. Inlet NO_x concentration *Y*: 800 ppm for pelletized catalysts, 400 ppm for monolith catalysts; inlet NO_x concentration (▪▪▪▪▪); outlet NO_x concentration (▬▬).

Table 2
Gas composition for sulfur-aging test, and NO_x storage measurement for monolithic catalysts.

Atmosphere	C_3H_6 (%C)	CO (%)	H_2 (%)	NO (ppm)	CO_2 (%)	SO_2 (ppm)	O_2 (%)	H_2O (%)	N_2 (%)
Sulfur-aging test									
Lean	0	0	0	0	11	50	6.5	3	Balance
Rich	0	6	2	0	11	0	0	3	Balance
NO_x storage measurement									
Lean	0.06	0	0	400	11	0	7	5	Balance
Rich/rich spike	0.32	6	1.6	400	11	0	0	5	Balance

3. Results and discussion

3.1. Effect of AZT calcination temperature on thermal stability

In order to confirm the most thermally stable AZT structure, five samples calcined at different final temperatures were synthesized. The specific surface areas (SSAs) of AZT calcined from 773 to 1173 K are shown in Table 3. These samples were evaluated as NSR catalysts composed of Pt/Rh/Ba/K/AZT*n* after thermal aging at 1073 K. The SSAs of catalysts after thermal aging are also shown in Table 3. Fig. 3 shows the NO_x storage capacities of pelletized catalysts at 573, 673 and 773 K after thermal aging. At 673 and 773 K, NSR performance is almost proportional to the size of SSA of catalysts after thermal aging. The P-AZT1073Cat shows the maximum NO_x storage especially at 673 and 773 K. This maximal storage capacity can be attributed to the structure of AZT1073, because structural changes tend to occur depending on the calcination temperature. Therefore, powder XRD patterns of AZT*n* were analyzed and these are shown in Fig. 4. The tetragonal ZrO_2 peak derived from ZT starts to appear weakly at 973 K, and then becomes clearly sharp at 1073 K or higher, demonstrating that ZT in AZT1073 is both crystallized completely and stable under high temperatures.

The crystallization of ZT has been reported to start at temperatures lower than 923 K, and catalysts containing ZT, which calcined at 923 K, have been shown to exhibit considerably high NO_x storage performance [25]. Therefore, since it could be inferred that the crystallization process for ZT in AZT was different to that in pure ZT, the XRD pattern of AZT1073 was compared with the pure ZT powder calcined from 873 to 1073 K. The XRD patterns around the tetragonal ZrO_2 (1 0 1) peak at $2\theta = 30.4^\circ$ of AZT 1073 and pure ZT are shown in Fig. 5. The particle size of ZT calculated

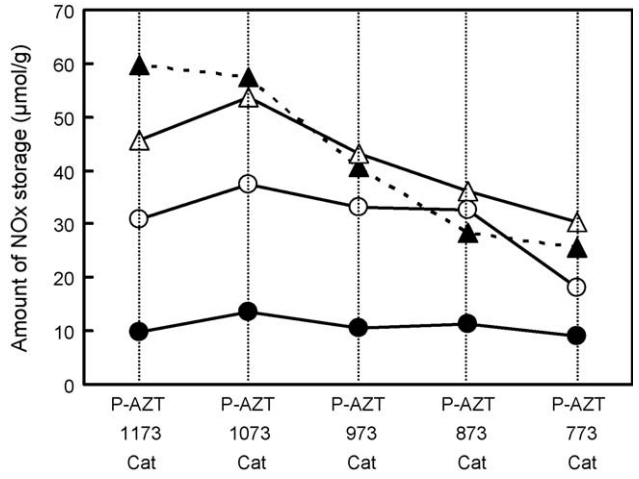

Fig. 3. NO_x storage using AZT catalysts after thermal aging as a function of specific surface area of supports. (●) NO_x storage measured at 573 K, (○) 673 K, (△) 773 K after thermal aging, and (▲) 773 K after sulfur aging.

Table 3
SSA of AZT*n* as prepared and their catalysts after thermal aging.

	Calcination temperature (K)	SSA (m^2/g)	SSA of catalyst after thermal aging (m^2/g)
AZT773	773	277	46.7
AZT873	873	224	50.0
AZT973	973	195	51.2
AZT1073	1073	128	58.1
AZT1173	1173	80	53.8

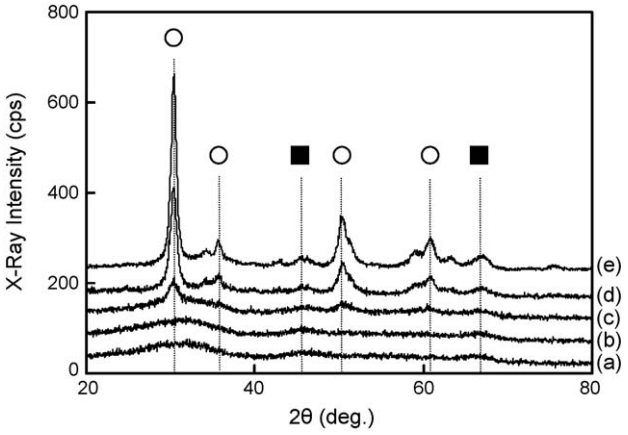

Fig. 4. XRD patterns of AZT at various calcination temperatures. (a) AZT773, (b) AZT873, (c) AZT973, (d) AZT1073, (e) AZT1173. (○) Tetragonal ZrO_2 and (■) γ-Al_2O_3.

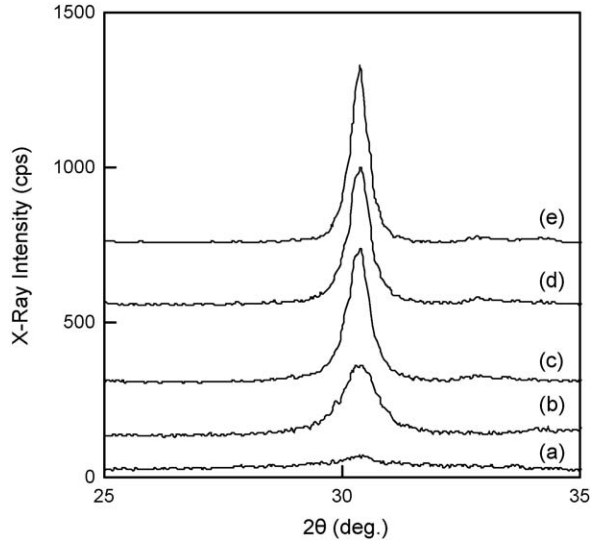

Fig. 5. XRD patterns of AZT1073 and a solid solution of pure ZrO_2–TiO_2 at various calcination temperatures. (a) 873 K, (b) AZT1073, (c) 923 K, (d) 973 K, and (e) 1073 K.

Table 4
Particle size of ZT calcined at various temperatures.

Temperature (K)	ZT particle size (nm)
1073 (AZT)	10
873	–
923	14
973	17
1073	24

from the XRD results is shown in Table 4. The particle size of ZT in AZT1073 is less than half of that of pure ZT calcined at the same temperature and corresponds to the particle size of pure ZT calcined between 873 and 923 K. These findings show that AZT1073 can be crystallized and that it forms a stable structure with maximal NSR performance. The small size of ZT corroborates the finding that AZT inhibits sintering of ZT [22], because Al_2O_3 acts as a diffusion barrier to ZT particles (Fig. 1). In AZT1173, although ZT has already crystallized, the SSA is 40% smaller than the AZT1073. Furthermore, the SSA of P-AZT1173Cat is also smaller than P-AZT1073Cat after thermal aging, as shown in Table 3. Once AZT has crystallized thoroughly, NSR performance is presumed to be proportional to the size of the SSA after thermal aging, as this affects the number of catalytic active sites.

Furthermore, the amount of NO_x storage of P-AZT1073Cat at 673 and 773 K is distinctly larger than that of other samples. The main reason of deactivation of storage materials after thermal aging is the deterioration of potassium, and potassium works as a NO_x storage material around this temperature region [26,27]. Compared with amorphous ZT, there is a possibility that crystallized ZT is stabilized, thus inhibiting the solid phase reaction with potassium. In order to confirm this point, the P-AZT1073Cat was selected for a crystallized AZT support, and the P-AZT773Cat for an amorphous AZT support. As a result, the ratio of solid phase-reacted potassium for the P-AZT1073Cat was 22%, whereas that of P-AZT773Cat was 52%. The primary source for the solid phase reaction with potassium is TiO_2 [7]. The ZT in AZT773 is amorphous and tends to induce a solid phase reaction with storage materials. Therefore, the initial reason for the high NSR performance of the P-AZT1073Cat at 773 K is the difference in the amount of deactivated potassium, because AZT1073 inhibits the reaction of storage materials with TiO_2 based on the crystallization of ZT. This result is also one of the reasons why P-AZT1073Cat has the largest SSA in spite of the same thermal aging condition for all samples.

Although the P-AZT1073Cat has the best NSR performance relative to thermal stability, it also requires durability with respect to sulfur if it is to be applied as an NSR catalyst. The NO_x storage capacities of catalysts using AZT calcined at different temperatures were measured after sulfur aging. The solid triangles joined by the dotted line in Fig. 3 show the amount of NO_x storage measured at 773 K after sulfur aging. The P-AZT1073Cat has a larger NO_x storage capacity than P-AZT773, 873 and 973Cats after sulfur aging. Sulfur durability is related to the basicity of supports [7], and acidic metal oxides with low basicity, such as TiO_2, show excellent sulfur durabilities due to the facilitation of the decomposition of sulfate materials [7,8]. AZT contains TiO_2 as ZrO_2–TiO_2 solid solution. However, basicity may change depending on the calcination temperature, followed by the change of the NSR performance. Using CO_2-TPD, the basicities of AZT773 and 1073 were determined to be 10.8 and 2.7 μmol/g, respectively. Therefore, the main reason of excellent NSR performance of the P-AZT1073Cat after sulfur aging is thought to be its low basicity.

These results suggest that AZT1073 is structurally well suited for NSR performance, exhibiting both thermal stability and sulfur durability. For this reason, AZT1073 was used as the standard AZT support in the following section.

3.2. Analysis of the AZT catalyst for sulfur durability

3.2.1. NSR performance after sulfur aging at high temperature

NSR catalysts become deactivated through the complex processes of thermal deterioration and sulfur poisoning. Therefore, monolithic catalysts were aged at 973 K or higher under the model exhaust gas atmosphere with SO_2, and exposed to a feed-stream alternating between rich and lean atmospheres to desorb and decompose the sulfur species. AZT is a nanocomposite of Al_2O_3 and ZT primary particles within the same secondary particle. Therefore, a catalyst with a physical mixture of Al_2O_3 and ZT as a support was selected as the reference catalyst to confirm the effect of the nanocomposite structure of AZT on sulfur durability.

Fig. 6 shows the NO_x storage capacity measured at 673 K in the monolithic AZT catalyst and the physically mixed catalyst after sulfur aging at 973, 1023, and 1073 K. The AZT catalyst has a larger NO_x storage capacity than the physically mixed catalyst at each temperature, although the amount of NO_x storage decreased with an increase in the aging temperature. This increased storage capacity was attributed to the unique structure of AZT. One such quality is the diffusion barrier of Al_2O_3 to ZT, which provides thermal stability [22] and low basicity for sulfur durability [18]. One critical difference observed between the AZT catalyst and the physically mixed catalyst can be seen in the deteriorated state of the NO_x storage materials, which, at 673 K, reflects the performance of both potassium and barium storage materials. Potassium stores NO_x as potassium nitrate above 623 K, whereas barium stores NO_x as barium nitrate in the low temperature region from 573 to 723 K [26,27]. Therefore, analysis and characterization of NO_x storage materials after aging must be conducted in order to understand the mechanism of optimal performance of the monolithic AZT catalyst.

3.2.2. Analysis of potassium species

The deteriorated states of NO_x storage materials were classified as the active state, which is capable of storing NO_x, the solid phase-reacted state, which arises due to the thermal reaction between storage materials and support materials, and the sulfate-formed state, which arises due to sulfur poisoning.

Table 5 shows the state of potassium in monolithic catalysts after aging at 1023 and 1073 K. The amount of active potassium in the AZT catalyst is larger than that in the physically mixed catalyst when samples were aged at 1023 K. The ratio of the solid phase-reacted potassium in the AZT catalyst is almost half that in the

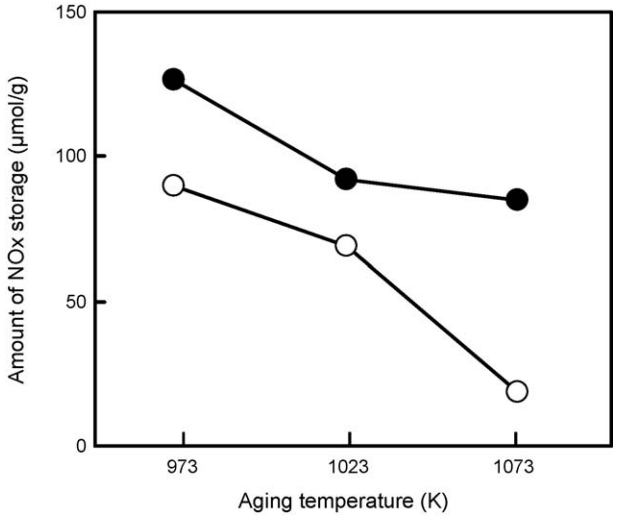

Fig. 6. NO_x storage after sulfur aging as a function of aging temperature. (●) Monolithic AZT catalyst and (○) monolithic physically mixed catalyst.

Table 5
The state of potassium in monolithic catalysts after sulfur-aging test at high temperature.

Sulfur-aging temperature	Catalyst	Active potassium (%)	Solid phase-reacted potassium (%)	Sulfate-formed potassium (%)
1023 K	AZT	84	9	7
	Physically mixed	78	17	5
1073 K	AZT	85	13	2
	Physically mixed	78	20	2

Table 6
The state of barium in monolithic catalysts after sulfur-aging test at high temperature.

Sulfur-aging temperature	Catalyst	Active barium (%)	Other barium (%)
1023 K	AZT	35	65
	Physically mixed	16	84
1073 K	AZT	31	69
	Physically mixed	22	78

physically mixed catalyst. Therefore, the primary reason for the large amount of active potassium in the AZT catalyst was attributed to the small amount of the solid phase-reacted potassium. This trend remained even after aging at 1073 K, and also led to high NO_x storage performance of the AZT catalyst. The AZT catalyst inhibits the formation of solid phase-reacted potassium at high temperatures, because the ZT phase has already been stabilized, as described in Section 3.1. The ratio of sulfate-formed potassium was relatively small for both samples, although the ratio decreased with an increase in aging temperature. Therefore, the primary reason for potassium deterioration at high temperatures was attributed to thermal deterioration, and the difference in the amount of solid phase-reacted potassium affected the NSR performance.

Interestingly, the EPMA results reveal that potassium species easily move to the monolith substrate in the physically mixed catalyst with an increase in the aging temperature. The physically mixed oxide has a broad pore distribution relative to AZT, and a macropore around 60 nm was observed after calcination at 1073 K due to the sintering of ZT. On the other hand, AZT was shown to form a single mesopore measuring approximately 15 nm [22]. These results indicate that potassium can easily move outside the catalyst layer and that the total amount of potassium species contained in the catalyst layer in the physically mixed catalyst was less than that added in catalyst preparation. This suggests that the amount of active potassium in the physically mixed catalyst is less than that shown in Table 5. This trend also contributes to the difference in the amount of NO_x storage for the AZT catalyst and the physically mixed catalyst.

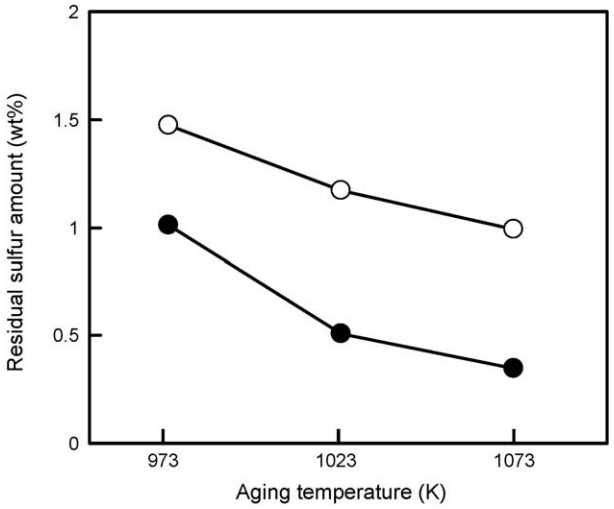

Fig. 7. Residual sulfur after sulfur aging as a function of aging temperature. (●) Monolithic AZT catalyst and (○) monolithic physically mixed catalyst.

3.2.3. Analysis of barium species

The state of barium in the samples after sulfur aging is shown in Table 6. The ratio of active barium in the AZT catalyst was larger than that in the physically mixed catalyst at both aging temperatures. Moreover, compared with the physically mixed catalyst, the AZT catalyst had twice the amount of active barium after aging at 1023 K effectively increasing the NO_x storage capacity of the AZT catalyst.

Further characterization of the barium species may be useful to elucidate the mechanism of action. In order to further examine the barium species, the sulfur species were identified because, as shown in Table 5, sulfur poisoning in potassium species is almost negligible. The adsorption of sulfur species on the support surface is thought to be negligible in this aging temperature region [8,18]. In addition, since the barium component in $Ba/CeO_2/Al_2O_3$ is also known to be selectively poisoned by sulfur [28], it is possible to consider that the difference in sulfur poisoning reflects the barium state for each catalyst.

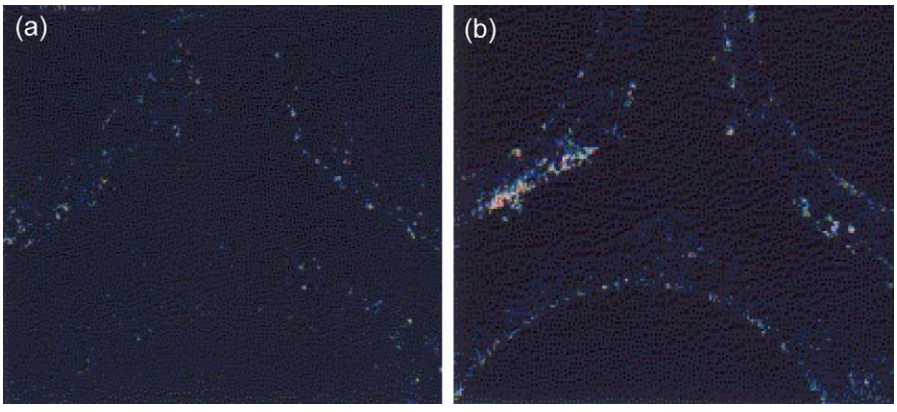

Fig. 8. EPMA images of S atom in the wash-coat layer after sulfur aging at 1023 K. (a) Monolithic AZT catalyst and (b) monolithic physically mixed catalyst.

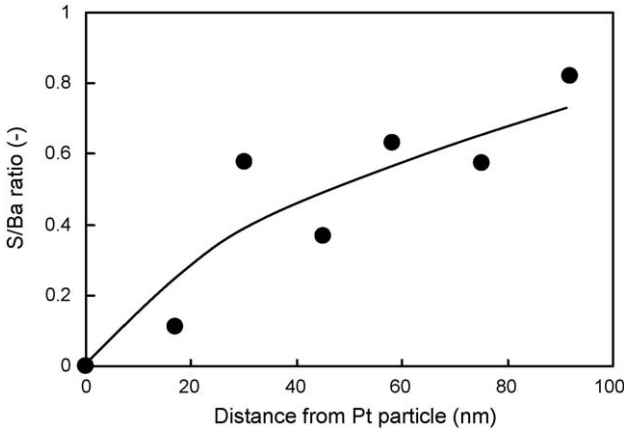

Fig. 9. Relationship between S/Ba ratio and distance from Pt particle in AZT catalyst after sulfur aging.

The residual sulfur after sulfur aging is shown in Fig. 7. The sulfur content in the AZT catalyst is less than that in the physically mixed catalyst. Specifically, the amount of sulfur in the AZT catalyst is less than half of that of the physically mixed catalyst at more than 1023 K. While sulfur was also observed in the catalysts layered on the monolithic substrate using EPMA (Fig. 8), almost no sulfur was detected in the AZT catalyst after the sulfur-aging test at 1023 K. The low basicity of the AZT surface facilitates facile desorption and degradation of sulfated materials during the alternating lean and rich atmosphere gas conditions [18]. Therefore, the difference in the basicities of AZT and the physically mixed oxide may be one reason why a large amount of active barium is maintained in the AZT catalyst.

Fig. 9 shows the sulfur to barium ratio in relation to the distance from a Pt particle observed in the AZT catalyst after the sulfur-aging test at 1023 K. The S/Ba ratio increases with distance from the Pt particle, because the decomposition of sulfates includes the reduction of SO_4^{2-} to SO_2, which is catalyzed by Pt [8]. In a previous study, the dispersion of noble metals in the AZT catalyst was reported to be twice that in the physically mixed catalyst after thermal aging at 1073 K [22]. This is because AZT inhibits sintering and aggregation of ZT and maintains a stable surface. Consequently, recovery from barium sulfate to active barium in NO_x storage is facilitated by the AZT support, which may contribute to the large amount of active barium in the monolithic AZT catalyst.

4. Conclusions

The effect of calcination temperature of AZT was investigated to assess the thermal stability of NSR catalysts. AZT calcined at 1073 K showed significant NO_x storage ability after thermal aging as a catalyst, because the ZT phase was already crystallized and thermally stable. Therefore, the solid phase reaction of potassium with support materials was inhibited, and a high ratio of active potassium remained in the AZT catalyst at 1073 K.

The AZT catalyst showed superior NO_x storage performance after sulfur aging at 973 K or higher compared to that of the physically mixed catalyst. The monolithic AZT catalyst inhibited the solid phase reaction of potassium with support materials and a high ratio of active potassium was maintained. In addition, barium in the AZT catalyst prevented sulfur poisoning and maintained NO_x storage based on low basicity and high Pt dispersion. Given the optimal balance that exists between thermal stability and sulfur durability, AZT calcined at 1073 K is a promising support for NSR catalysts.

Acknowledgements

The authors thank Mr. Yuzo Kawai for ICP analysis, Mr. Yasuhito Kondou for conducting the combustion infrared absorption analyses, and Ms. Kumi Amano for S atom mapping by EPMA.

References

[1] S. Sato, Y. Yu-u, H. Yahiro, N. Mizuno, M. Iwamoto, Appl. Catal. 70 (1991) L1.
[2] Y. Kintaichi, H. Hamada, M. Tabata, M. Sasaki, T. Ito, Catal. Lett. 6 (1990) 239.
[3] R. Burch, P.J. Millington, Catal. Today 26 (1995) 185.
[4] T. Ishihara, M. Ando, K. Sada, K. Takiishi, K. Yamada, H. Nishiguchi, Y. Takita, J. Catal. 220 (2003) 104.
[5] N. Miyoshi, S. Matsumoto, K. Katoh, T. Tanaka, J. Harada, N. Takahashi, K. Yokota, M. Sugiura, K. Kashahara, SAE Paper 950809, 1995.
[6] N. Takahashi, H. Shinjoh, T. Iijima, T. Suzuki, K. Yamazaki, K. Yokota, H. Suzuki, N. Miyoshi, S. Matsumoto, T. Tanizawa, T. Tanaka, S. Tateishi, K. Kasahara, Catal. Today 27 (1996) 63.
[7] N. Takahashi, A. Suda, I. Hachisuka, M. Sugiura, H. Sobukawa, H. Shinjoh, Appl. Catal., B: Environ. 72 (2006) 187.
[8] S. Matsumoto, Y. Ikeda, H. Suzuki, M. Ogai, N. Miyoshi, Appl. Catal., B: Environ. 25 (2000) 115.
[9] E.C. Corbos, X. Courtois, N. Bion, P. Marecot, D. Duprez, Appl. Catal., B: Environ. 80 (2008) 62.
[10] X. Wei, X. Liu, M. Deeba, Appl. Catal., B: Environ. 58 (2005) 41.
[11] J. Dawody, M. Skoglundh, L. Olsson, E. Fridel, Appl. Catal., B: Environ. 70 (2007) 179.
[12] Z. Liu, J. Anderson, J. Catal. 228 (2004) 243.
[13] J.H. Kwak, D.H. Kim, J. Szanyi, C.H.F. Peden, Appl. Catal., B: Environ. 84 (2008) 545.
[14] S. Hammache, L.R. Evans, E.N. Coker, J.E. Miller, Appl. Catal., B: Environ. 78 (2008) 315.
[15] K. Yamamoto, R. Kikuchi, T. Takeguchi, K. Eguchi, J. Catal. 238 (2006) 449.
[16] T. Kanazawa, Catal. Today 96 (2004) 171.
[17] K. Ito, S. Kakino, K. Ikeue, M. Machida, Appl. Catal., B: Environ. 74 (2007) 137.
[18] H. Imagawa, T. Tanaka, N. Takahashi, S. Matsunaga, A. Suda, H. Shinjoh, Appl. Catal., B: Environ. 86 (2009) 63.
[19] K.M. Adams, G.W. Graham, Appl. Catal., B: Environ. 80 (2008) 343.
[20] M. Casapu, J. Grunwaldt, M. Maciejewski, M. Wittrock, U. Göbel, A. Baiker, Appl. Catal., B: Environ. 63 (2006) 232.
[21] N. Takahashi, S. Matsunaga, T. Tanaka, H. Sobukawa, H. Shinjoh, Appl. Catal., B: Environ. 77 (2007) 73.
[22] H. Imagawa, T. Tanaka, N. Takahashi, S. Matsunaga, A. Suda, H. Shinjoh, J. Catal. 251 (2007) 315.
[23] J.A. Anderson, R.A. Daley, S.Y. Christou, A.M. Efstathiou, Appl. Catal., B: Environ. 64 (2006) 189.
[24] N. Takahashi, K. Yamazaki, H. Sobukawa, H. Shinjoh, J. Chem. Eng. Jpn. 39 (2006) 437.
[25] Y. Liu, M. Meng, X.G. Li, L.H. Guo, Y.Q. Zha, Chem. Eng. Res. Des. 86 (2008) 932.
[26] I. Hachisuka, T. Yoshida, H. Ueno, N. Takahashi, A. Suda, S. Sugiura, SAE Paper 2002-01-0732, 2002.
[27] M. Takeuchi, S. Matsumoto, Top. Catal. 28 (2004) 151.
[28] F. Rohr, S.D. Peter, E. Lox, M. Kögel, A. Sassi, L. Juste, C. Rigaudeau, G. Belot, P. Gelin, M. Primet, Appl. Catal., B 56 (2005) 201.